Compensating commutation-angle domain disturbances with application to waveform optimization for piezo stepper actuators

Aarnoudse, Leontine; Strijbosch, Nard; Tacx, Paul; Verschueren, Edwin; Oomen, Tom

DOI
10.1016/j.mechatronics.2023.103016

Publication date
2023

Document Version
Final published version

Published in
Mechatronics

Mechatronics 94 (2023) 103016

Contents lists available at ScienceDirect

Mechatronics

journal homepage: www.elsevier.com/locate/mechatronics

Compensating commutation-angle domain disturbances with application to waveform optimization for piezo stepper actuators☆,☆☆

Leontine Aarnoudse [a,*,1], Nard Strijbosch [b,1], Paul Tacx [a,1], Edwin Verschueren [c,1], Tom Oomen [a,d,1]

[a] Department of Mechanical Engineering, Control Systems Technology, Eindhoven University of Technology, Eindhoven, The Netherlands
[b] IBS Precision Engineering, Eindhoven, The Netherlands
[c] Thermo Fisher Scientific, Eindhoven, The Netherlands
[d] Delft Center for Systems and Control, Delft University of Technology, Delft, The Netherlands

ARTICLE INFO

Keywords:
Iterative learning control
Feedforward control
Piezo actuators

ABSTRACT

Piezo stepper actuators are very promising for nanopositioning systems due to their high resolution, high stiffness, fast response, and the ability to position a mover over an infinite stroke by means of motion reminiscent of walking. The aim of this paper is to enhance the waveforms for actuating piezo steppers, by actively compensating for repetitive disturbances that are introduced by the walking behavior. A compensation method is developed to compensate for disturbances in the stepping domain, since disturbances may vary in the time domain if the velocity changes. The results from this procedure are exploited to determine an optimal waveform for the working range of the actuator. A significant improvement in performance is achieved after applying this waveform to a piezo stepper actuator.

1. Introduction

Piezo actuators are a promising technique for high precision motion systems, especially since "walking" enables long-stroke actuation. Applications such as nano-motion stages [1] and scanning probe microscopes [2] require actuators with high accuracy, high stiffness, fast response, and a large stroke. Individual piezoelectric elements meet the high accuracy, high stiffness and fast response time requirements, yet their stroke is limited. Piezo stepper actuators can meet the additional requirement of a large stroke through a motion that resembles walking. There are various ways to implement this walking motion, for example by walking drives [3] or bi-morph legs [4].

The walking behavior is implemented through waveforms, which define the input to the individual piezo elements as a function of the commutation angle, α, see, e.g., [5]. A full step of the piezo stepper actuator is defined on the interval $\alpha \in [0, 2\pi)$ and extends periodically. The control input is given by the step frequency f_α, in steps per second, which is integrated to obtain the commutation angle that dictates the walking behavior.

During the walking motion of a piezo stepper actuator, engagement and release between the piezo elements and the mover can lead to repeating disturbances. These disturbances lead to a nonlinear relation between the commutation angle and the position output, which is limiting for control. Experiments reveal that these disturbances are highly reproducible with respect to the commutation angle [6]. Since piezo stepper actuators typically operate with varying velocities, these periodic disturbances in the commutation angle domain typically lead to a non-periodic error in the temporal domain.

The design of the input waveforms is essential to achieve high performance. In [7] a procedure is outlined to optimize the waveform to obtain the highest possible speed with a piezo stepper actuator. In [1], both model-based and data-based optimization algorithms are introduced that minimize the velocity error when applying a constant drive frequency. Both methods lead to an optimal waveform for a specific velocity, without guarantees for other velocities. Besides this, these methods do not exploit the reproducibility of the disturbances. In [4], a model-based coordinate transformation is used to define the waveforms for a piezo LEGS actuator based on the desired step shape. The resulting waveforms do not compensate for the unmodeled repeating disturbances due to engagement and release. In [8], two parameters of the contact dynamics are estimated iteratively to increase

☆ This work is part of the research programme VIDI with project number 15698, which is (partly) financed by the NWO.
☆☆ This paper was recommended for publication by Associate Editor Zheng Chen.
* Corresponding author.
E-mail address: l.i.m.aarnoudse@tue.nl (L. Aarnoudse).
[1] All authors contributed with initial ideas and writing comments on the whole manuscript. The final author is the principal investigator.

https://doi.org/10.1016/j.mechatronics.2023.103016
Received 16 February 2023; Received in revised form 26 April 2023; Accepted 9 June 2023
Available online 26 June 2023

the smoothness of the takeovers in a piezo stepper, reducing the 'hammering' effect in vertical direction during horizontal motion. In [2], disturbances caused by the takeover between leg pairs are reduced by inputs that ensure a gradual takeover, during which both leg pairs move with the same velocity. For the piezo stepper actuator considered in this paper, the waveforms ensure such a gradual takeover during which the elements in contact with the mover move with equal velocity, yet this does not fully eliminate the disturbances.

Several approaches to iterative learning control outside the temporal domain have been developed, see, e.g., [9–11]. In [9], temporal dynamics are ignored to obtain a static system in the time domain, which is exploited in a 2D spatial ILC approach. This method is developed for additive manufacturing systems where the output of the system is measured at a fixed number of equidistant discrete points in the spatial domain. However, for piezo steppers the commutation angle can take any value in a continuous interval. In [10], an ILC approach is developed that indexes previous iterations of a bipedal walking robot by a phase variable reminiscent of the commutation angle of a piezo stepper actuator. This method assumes that stable periodic walking with an unknown period time is obtained in the limit. For piezo stepper actuators, this assumption is not valid as the input drive frequency typically leads to various velocities, i.e., varying period times. In [11], a repetitive control approach is developed to compensate for disturbances in the position domain. This approach uses Gaussian processes to interpolate between the non-equidistantly sampled data points. Due to the heavy computational load required to compute the posterior distribution of the Gaussian process, this cannot directly be applied to the design of waveforms for piezo stepper actuators.

Although several waveform optimization techniques have been developed, a procedure that exploits the reproducible disturbances in the commutation angle domain is lacking. Consequently, for each of these methods an error will remain that can be compensated for through learning. The aim of this paper is to develop a computationally tractable, data driven optimization approach to enhance piezo stepper waveforms. Through learning from error data of past step cycles a waveform is determined that compensates for all disturbances related to the walking behavior, and that is parameterized by only a few parameters. Implementation of this waveform leads to a linear relation between the commutation angle input and the position output. The contribution of this paper consists of the following steps.

- S1 A disturbance analysis, which reveals that the disturbances that effect a piezo stepper are highly reproducible in the commutation angle domain (Section 3).
- S2 A waveform optimization algorithm that mitigates the reproducible part of these disturbances by iteratively updating the waveforms while allowing for a varying step frequencies (Section 4).
- S3 Implementation of the framework on a piezo stepper actuator (Section 5).

Preliminary results of the research presented here are reported in [6,12]. In [12] an iterative waveform optimization procedure is introduced without considering sampling of the measurement signals, and learning is only applied during so-called 'clamping' experiments and not during the actual walking motion of the piezo stepper actuator. In [6], the non-equidistant sampling of the error is addressed using radial basis functions and the algorithm is implemented during normal operation modes, i.e., 'walking'. The current paper presents a unifying framework that includes periodic basis functions, which are more suitable given the nature of the disturbance. Moreover, all proofs are included.

2. Problem formulation

In this section, the problem considered in this paper is introduced. First, piezo stepper actuators are introduced. Secondly, the typical design of the waveforms is illustrated. Thirdly, some assumptions on the disturbances are given and lastly the considered problem is formulated.

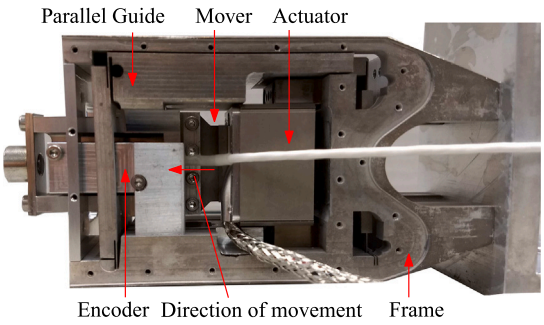

Fig. 1. Experimental setup with piezoelectric actuator.

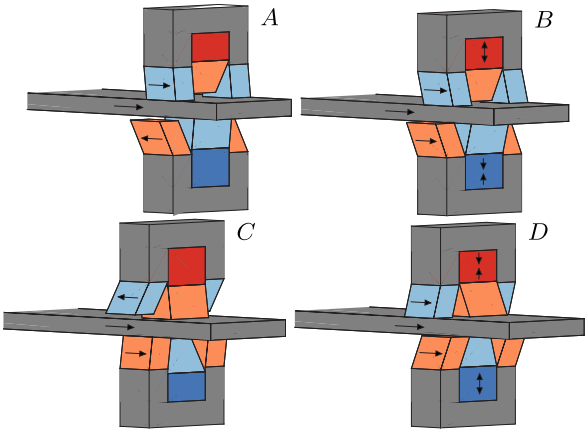

Fig. 2. Schematic representation of piezo stepper actuator in each of the four phases of a stepping motion. The different piezo elements are: longitudinal piezo of group 1 ( ); longitudinal piezo of group 2 ( ); shear piezo of group 1 ( ); shear piezo of group 2 ( ).

2.1. Piezo stepper actuators

Piezo stepper actuators consist of a combination of piezoelectric elements in varying configurations that propel a mover, see, e.g., [3,4]. In the piezo stepper actuator considered in this paper, see Fig. 1, the piezoelectric elements are configured as schematically depicted in Fig. 2. The actuator consists of two groups of piezo elements, each containing a longitudinal element that can extend perpendicular to the mover, and three shear elements that can extend in the direction of the movement. When the longitudinal element of a group is extended, the corresponding shear elements are in contact with the mover and dictate the position of the mover. The two piezo groups are alternated to obtain a walking motion, leading to an unlimited stroke of the mover.

The walking behavior is dictated by a set of waveforms that define the relationship between the inputs of the individual piezo elements. The design of these waveforms is crucial to achieving high performance. The waveforms map the commutation angle $\alpha \in \mathbb{R}$ to the input voltages for the longitudinal piezo elements, c_1 and c_2, and the sets of shear piezo elements, s_1 and s_2. They are defined on the interval $\alpha \in [0, 2\pi)$ and extend periodically. A full cycle from $\alpha = 0$ to $\alpha = 2\pi$ corresponds to a step of the first piezo group followed by a step of the second piezo group.

The waveforms are implemented as shown in Fig. 3, with output y [m] the position of the mover and input f_α [Hz] the step frequency, which is defined as the number of step cycles of the piezo stepper actuator per time unit. The commutation angle α [rad] is defined as

$$\alpha(t) = 2\pi \int_0^t f_\alpha(\tau)\mathrm{d}\tau. \tag{1}$$

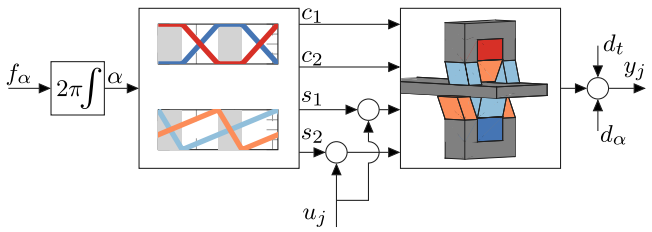

Fig. 3. Open-loop implementation of waveforms to actuate the piezo stepper actuator. From the input f_α (step frequency) to the output y_j (Mover position).

The commutation angle α [rad] over time for a given step frequency f_α [Hz] is illustrated in Fig. 5.

2.2. Waveform design

A typical waveform design is shown in Fig. 4. This set of waveforms is designed to obtain a linear relation between the commutation angle α [rad] and the position y [m], i.e.,

$$y_d(t) = \kappa\alpha(t) = \kappa 2\pi \int_0^t f_\alpha(\tau)\mathrm{d}\tau, \tag{2}$$

where the constant κ [m/rad] is the desired step size, which depends on the piezoelectric material and the size of the piezo element. The waveforms for the longitudinal piezo elements are designed to obtain four distinct phases.

(A) Shear piezo elements of group 1 in contact with the mover, shear piezo elements of group 2 not in contact with the mover.
(B) Transition phase.
(C) Shear piezo elements of group 1 not in contact with the mover, shear piezo elements of group 2 in contact with the mover.
(D) Transition phase.

The waveform design for the shear piezo elements exploits these phases to propel the mover forward. In the phases in which the shear piezo elements of a group are in contact with the mover, they move in the direction of the mover. The phase in which the shear piezo elements of one group are not in contact with the mover is exploited to reset these elements, i.e., move in the opposite direction of the mover. This waveform design is based on a model of the piezoelectric shear elements given by

$$y_s(t) = cu_s(t), \tag{3}$$

with $y_s(t)$ [m] the displacement of the shear piezo element, $u_s(t)$ [V] the applied voltage, and c [m/V] a material-dependent constant. This model leads to the waveforms depicted in Fig. 4. The desired behavior for the position y and velocity $\dot{y}$ is depicted in Fig. 5.

One of the key properties of the model (3) is its static behavior, i.e., both in the temporal and commutation angle domain the system is linear and shift invariant. Piezoelectric elements are well known to suffer from hysteresis and creep effects. However, these effects are omitted in (3), since they are well understood in literature and can be compensated for, see, e.g., [13–15]. This is formalized in the next assumption.

Assumption 1. It is assumed that hysteresis, creep and possible drift effects are appropriately addressed. This enables the use of the piezoelectric model (3).

2.3. Disturbances

Disturbances are inevitable in an experimental setting. For the piezo stepper actuator, these disturbances could have different sources. For

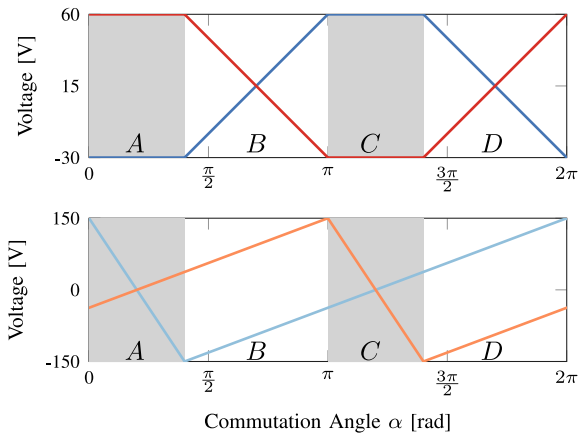

Fig. 4. Top: waveforms applied to clamping piezo elements, $c_1(\alpha)$ (—), $c_2(\alpha)$ (—). Bottom: waveforms applied to shear piezo elements, $s_1(\alpha)$ (—), $s_2(\alpha)$ (—). Interval A indicates the interval where the longitudinal piezo element of group 2 is fully extended and the shears of group 1 are not in contact with the mover. Interval C indicates the interval where the longitudinal piezo element of group 1 is fully extended and the shears of group 2 are not in contact with the mover. Intervals B and D indicate the transition intervals.

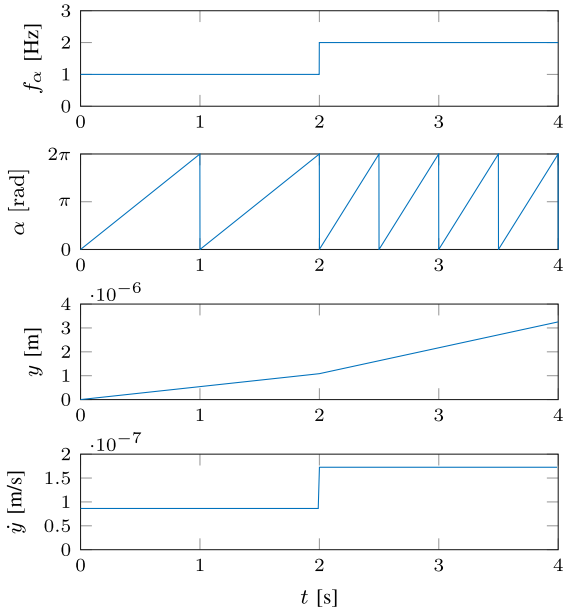

Fig. 5. Desired commutation angle $\alpha(t)$, position $y(t)$, and velocity $\dot{y}(t)$ when applying the input signal $f_\alpha(t)$ to a piezo stepper actuator.

example, a longitudinal piezo element that is not perfectly perpendicular to the mover can cause a disturbance force in the direction of the movement. In addition, contact dynamics can influence the position when the shear elements come in contact with the mover [8]. Variations in the properties of the piezo elements can cause differences in the velocities of the piezo elements. Moreover, sensor noise influences the measured position.

These disturbances are modeled by two lumped disturbances $d_\alpha(\alpha)$ and $d_t(t)$. The disturbance d_α captures all disturbances that can be directly related to the commutation angle. All other disturbances are captured by d_t. Throughout this paper, the following is assumed.

Assumption 2. Disturbance d_α is dominant compared to disturbance d_t, i.e., $\|d_\alpha\| \gg \|d_t\|$.

The validity of this assumption is assessed in Section 3. Using Assumption 2, the position of the mover can be written as

$$y(t) = \kappa\alpha(t) + d_\alpha(\alpha(t)). \tag{4}$$

2.4. Problem formulation

The aim of this paper is to enhance piezo stepper actuator waveforms by including compensation for the disturbance d_α. To this end, a learning algorithm is developed that employs past commutation-domain error signals. This learning algorithm can enhance the waveforms to compensate for the disturbances in a piezo stepper actuator due to their reproducible nature in the commutation angle domain. The approach encompasses

- modeling the piezo stepper in the commutation angle domain,
- dealing with non-equidistant sampling in the commutation angle domain, and
- translating the result into an optimized waveform.

3. Disturbance analysis

In this section, the validity of Assumption 2 is experimentally assessed. A set of open-loop walking experiments is performed on a piezo stepper actuator, configured as in Fig. 2, to identify the disturbances d_α and d_t.

Definition 1 (*Open-loop Walking Experiment*)**.** A signal $f_\alpha(t)$ is applied in the open-loop control configuration as depicted in Fig. 3. The displacement of the mover is measured.

This experiment is repeated for a wide variety of input signals $f_\alpha(t)$, resulting in the position outputs shown in Fig. 6. The error is defined as $e(t) = y_d(t) - y(t)$, with $y_d(t) = \kappa\alpha(t)$ and $\kappa = 3 \cdot 10^{-7}$ according to (2). To further analyze the disturbances in both the temporal domain and the α-domain for varying frequencies, the slope of the error signals is removed, resulting in the trendline deviation e_{td}, as shown in Fig. 7. In the α-domain, a clear correlation between these error signals for different experiments is visible, see Fig. 7 (bottom). This figure also illustrates that the error component e_{td} is clearly periodic, which influences the choice of basis functions in Section 4. There is no correlation between the errors of the experiments when evaluated in the temporal domain, see Fig. 7 (top). The same effect is visible in Fig. 6. Based on this observation, Assumption 2 is assumed to hold. This constitutes Step S1 of this paper.

Remark 2. Due to the equidistant sampling of the error signal in the temporal domain, the error signals that are mapped to the α-domain are non-equidistant in the α-domain when the step frequency varies. This motivates the introduction of basis functions in Section 4.3.

This insight on the reproducibility of the disturbance in the commutation angle domain is exploited in the next section to determine a data-driven waveform optimization algorithm that compensates for the disturbance.

4. Waveform optimization

In this section, a waveform optimization procedure is developed that can compensate for disturbances that are reproducible in the commutation angle domain. The key idea of this procedure is to exploit the error e_j at iteration j to determine a correction u_{j+1} for the waveforms, see Fig. 3, that mitigates this error in the next iteration. To determine a continuous signal u_{j+1}, the non-equidistantly sampled measurements of the error $\bar{e}_j$ are projected on a set of continuous basis functions. First, the procedure is summarized. In the remainder of the section, all steps are detailed and proved.

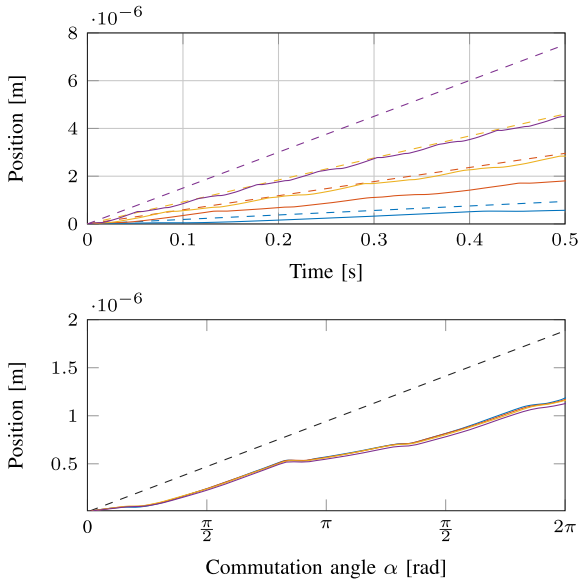

Fig. 6. Position for a piezo stepper during open-loop walking with step frequencies 1 Hz (—), π Hz (—), $2\sqrt{6}$ Hz (—) and 8 Hz (—). The dashed lines indicate the reference $y_d(\alpha)$ at the various drive frequencies.

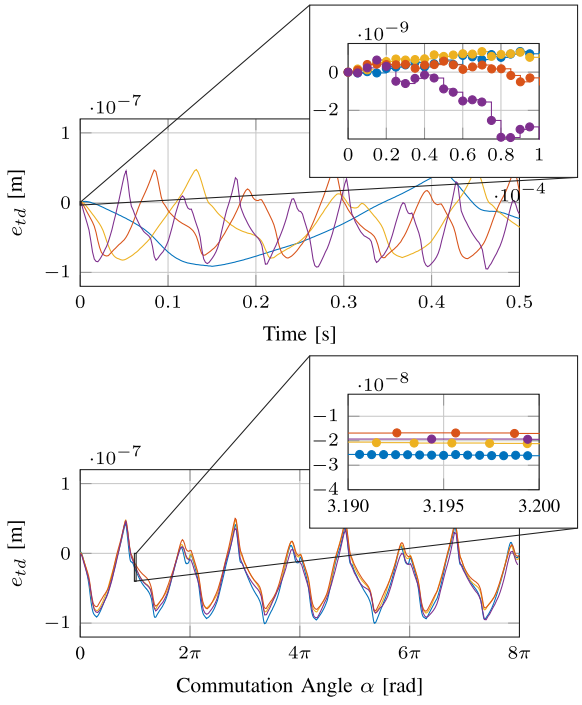

Fig. 7. Disturbances for a piezo stepper without slope during open-loop walking with step frequencies 1 Hz (—), π Hz (—), $2\sqrt{6}$ Hz (—) and 8 Hz (—). The sampling instances are indicated by dots (•). In the temporal domain (top) the sampling is equidistant (see zoom plot), but the disturbance is not repeating for different step frequencies. In the α-domain (bottom) the disturbances are highly reproducible, but the sampling instances vary depending on the step frequency.

Procedure 1 (*Iterative Waveform Optimization*).

1. Perform an experiment j with shear waveforms $s_{1,j}$ and $s_{2,j}$ and collect the sampled measurement data $\bar{e}_j(\bar{\alpha})$, $\bar{\alpha} = \{\bar{\alpha}_1, \bar{\alpha}_2, \dots, \bar{\alpha}_N\}$.
2. Reconstruct the continuous signal $e_j(\alpha)$, $\alpha \in [0, 2\pi)$, using basis functions, see Section 4.3.
3. Determine an input $u_{j+1}(\alpha)$, $\alpha \in [0, 2\pi)$, for the shear piezo elements, s_1 and s_2, that aims to mitigate the error $e_j(\alpha)$, see Sections 4.2 and 4.3.
4. From the input u_{j+1} construct updated waveforms $s_{1,j+1}$ and $s_{2,j+1}$, see Section 4.4.
5. Increase $j+1$ and repeat from step 1 with the updated waveforms.

Next, Steps 2–4 of Procedure 1 are developed. First, a set of assumptions is imposed. Secondly, the waveform update law for the input u_{j+1} is introduced, constituting Step 3, and conditions that guarantee convergence are provided. A projection-based algorithm is introduced to reconstruct the continuous error signal based on the available intermittently sampled version, constituting Step 2. Finally, a procedure is outlined that constructs updated waveforms $s_{1,j+1}$ and $s_{2,j+1}$ from the input u_{j+1}, constituting Step 4.

4.1. Assumptions

The following set of assumptions is imposed.

Assumption 3. The position $y_j(0)$ is identical for each experiment.

This ensures that each experiment starts from identical conditions.

Assumption 4. Each trial is of constant length in the commutation angle domain, i.e., $\alpha_j \in [0, 2\pi)$.

This ensures that all experiments have the complete information of the disturbance.

Assumption 5. The disturbances affecting the system are iteration-invariant in the commutation angle domain.

These assumptions enable iterative learning of a signal that compensates for the reproducible disturbance. The set of assumptions is reminiscent of the standard assumptions imposed in iterative learning control, where compensating signals are computed for systems with repeating disturbances in the temporal domain. Assumption 3 is equivalent to the standard equivalent initial condition assumption in traditional ILC. Assumption 4 is an adaptation of the constant time length assumption in traditional ILC. Note that Assumption 4 could lead to experiments with varying time lengths, since varying step frequencies lead to varying time lengths to complete a full step. Assumption 5 is equivalent to the assumption of iteration-invariant disturbances in the temporal domain in traditional ILC.

4.2. Learning update

In order to introduce a learning update, it is assumed that Step 2 and Step 4 are performed correctly. First, an additional input to the shear piezo elements is introduced, u_j in Fig. 3. This additional input signal is used to compensate for the observed disturbances. Exploiting the model of the shear piezo elements, (3), the model of the piezo stepper (4) is extended to

$$y_j(t) = \kappa\alpha(t) + d_\alpha(\alpha(t)) + cu_j(\alpha(t)). \tag{5}$$

The linear relation between the input u_j and the output in the temporal domain enables a simple conversion of this model to the commutation angle domain, given by

$$y_j(\alpha) = \kappa\alpha + d_\alpha(\alpha) + cu_j(\alpha). \tag{6}$$

The error in the commutation angle domain is now defined as

$$e_j(\alpha) = y_d(\alpha) - y_j(\alpha) = -cu_j(\alpha) - \hat{d}_\alpha(\alpha), \tag{7}$$

with $\hat{d}_\alpha(\alpha) = y_d(\alpha) - \kappa\alpha - d(\alpha)$ a lumped disturbance in the commutation angle domain. The goal of the waveform optimization algorithm is to minimize this error, i.e., to determine $u_j(\alpha)$ such that it perfectly compensates for the disturbance $\hat{d}_\alpha(\alpha)$.

The following update law is introduced to update the input u_j.

$$u_{j+1}(\alpha) = u_j(\alpha) + \gamma e_j(\alpha), \tag{8}$$

with gain $\gamma \in \mathbb{R}$. The design problem now reduces to selecting $\gamma \in \mathbb{R}$ such that the sequence of errors $\{e_j\}_{j\in\mathbb{Z}_{\geq 0}}$ converges to a unique and small e_∞.

Remark 3. The update law (8) is reminiscent of a *P*-type ILC update law [16]. Since the behavior of a piezo stepper actuator (2) can be modeled by a gain, P-type ILC is equivalent to inverse-model ILC.

Substituting (7) into (8) yields the following closed-loop trial domain dynamics of the sequence of input signals $\{f_j\}_{j\in\mathbb{Z}_{\geq 0}}$.

$$u_{j+1}(\alpha) = (1 - \gamma c)u_j(\alpha) - \gamma\hat{d}_\alpha(\alpha). \tag{9}$$

These iteration domain dynamics lead to the following convergence result.

Theorem 4. *Consider system (7) satisfying Assumptions 3–5 and update law (8). Then the sequence of input signals $\{u_j\}_{j\in\mathbb{Z}_{\geq 0}}$ converges monotonically to a unique $u_\infty(\alpha) = \frac{1}{c}\hat{d}_\alpha(\alpha)$ if and only if $0 < \gamma < \frac{2}{c}$. Moreover, $e_\infty(\alpha) = 0$.*

Theorem 4 leads to a straightforward design of the update law (8) when an approximation of c is available.

4.3. Signal parameterization

The learning update (8) hinges upon the availability of continuous signals. Besides the required continuous-time error signal, the control input u_j is also defined as a continuous signal. In a digital control implementation, obtaining these continuous signals is not possible. Therefore, continuous functions are introduced that approximate the required signals.

Typically the measurement signals are sampled equidistantly in the temporal domain, i.e., a continuous-time signal $y(t)$, $t \in \mathbb{R}_{\geq 0}$ is sampled to obtain a discrete measurement signal $y_{dt}(k)$, $k \in \mathbb{Z}_{\geq 0}$ as

$$y_{dt}(k) = y(kh) \tag{10}$$

with $h \in \mathbb{R}_{>0}$ the sampling time. For varying step frequencies, this equidistant sampling in the temporal domain leads to iteration-varying, non-equidistantly sampled measurement data in the commutation angle domain, see Fig. 7. To overcome this issue, an approximation of the continuous signal in the commutation angle domain is constructed by projecting the available non-equidistant data points on a set of continuous basis functions. The error signal is parameterized as follows.

$$e_j(\alpha) = \begin{bmatrix}\phi_1(\alpha) & \phi_2(\alpha) & \dots & \phi_m(\alpha)\end{bmatrix}\theta_j^e, \tag{11}$$

with $m \in \mathbb{N}$ linearly independent basis functions and parameters θ_{ji}^e, $i \in \{1, 2, \dots, m\}$.

This parameterization also enables the implementation of u_j as a continuous signal parameterized by the continuous basis functions ϕ_i, $i \in \{1, \dots, m\}$. To this end, Procedure 1 is started with an input signal u_0 that is parameterized by the basis functions ϕ_i, $i \in \{1, \dots, m\}$, i.e., $u_0(\alpha) = \begin{bmatrix}\phi_1(\alpha) & \phi_2(\alpha) & \dots & \phi_m(\alpha)\end{bmatrix}\theta_0^u$ for some θ_0^u. The update law (8) then yields the following

$$\begin{aligned} u_1 &= \begin{bmatrix}\phi_1(\alpha) & \phi_2(\alpha) & \dots & \phi_m(\alpha)\end{bmatrix}\theta_0^u \\ &\quad + \gamma\begin{bmatrix}\phi_1(\alpha) & \phi_2(\alpha) & \dots & \phi_m(\alpha)\end{bmatrix}\theta_0^e, \\ &= \begin{bmatrix}\phi_1(\alpha) & \phi_2(\alpha) & \dots & \phi_m(\alpha)\end{bmatrix}(\theta_0^u + \gamma\theta_0^e). \end{aligned} \tag{12}$$

From this it follows that all subsequent input signals generated by the update law (8) can be parameterized by the basis functions ϕ_i, $i \in \{1, \dots, m\}$, i.e., $u_j(\alpha) = \begin{bmatrix}\phi_1(\alpha) & \phi_2(\alpha) & \dots & \phi_m(\alpha)\end{bmatrix} \theta_j^u$ for all $j \in \mathbb{Z}_{\geq 0}$.

To find the correct parameters θ_j^e given θ_0^e, the following assumption is imposed.

Assumption 6. Given $\hat{d}_\alpha$ and ϕ_i, $i \in \{1, \dots, m\}$, there exist a $\theta^d \in \mathbb{R}^m$ such that

$$\hat{d}_\alpha(\alpha) = \begin{bmatrix}\phi_1(\alpha) & \phi_2(\alpha) & \dots & \phi_m(\alpha)\end{bmatrix} \theta^d. \tag{13}$$

Using this assumption, the error $e_j(\alpha)$ given in (7) is written as

$$\begin{aligned} e_j &= -c \begin{bmatrix}\phi_1(\alpha) & \phi_2(\alpha) & \dots & \phi_m(\alpha)\end{bmatrix} \theta_j^u \\ &\quad - \begin{bmatrix}\phi_1(\alpha) & \phi_2(\alpha) & \dots & \phi_m(\alpha)\end{bmatrix} \theta^d, \\ &= \begin{bmatrix}\phi_1(\alpha) & \phi_2(\alpha) & \dots & \phi_m(\alpha)\end{bmatrix} (-c\theta_j^u - \theta^d). \end{aligned} \tag{14}$$

This leads to the following result.

Theorem 5. *Consider the continuous error signal $e_j(\alpha)$, as given in (14), and its sampled version $\bar{e}_j = \begin{bmatrix}e_j(\alpha_1) & e_j(\alpha_2) & \dots & e_j(\alpha_N)\end{bmatrix}$ with $\alpha_i \in [0, 2\pi)$, $i \in \{1, \dots, N\}$ the commutation angle at the $N \in \mathbb{N}$ measurement instances obtained during a walking experiment with possibly varying step frequency. In addition, let matrix*

$$\boldsymbol{\Phi}_j = \begin{bmatrix} \phi_1(\alpha_1) & \phi_2(\alpha_1) & \dots & \phi_m(\alpha_1) \\ \phi_1(\alpha_2) & \phi_2(\alpha_2) & \dots & \phi_m(\alpha_2) \\ \vdots & \vdots & \vdots & \vdots \\ \phi_1(\alpha_N) & \phi_2(\alpha_N) & \dots & \phi_m(\alpha_N) \end{bmatrix}. \tag{15}$$

Then, the continuous error signal e_j can be exactly reconstructed if there are at least m unique sampling instances α_i, i.e., $N \geq m$. Moreover, this exact reconstruction is given by

$$e_j(\alpha) = \begin{bmatrix}\phi_1(\alpha) & \phi_2(\alpha) & \dots & \phi_m(\alpha)\end{bmatrix} \theta_j^e \tag{16}$$

with $\theta_j^e = \begin{bmatrix}\theta_{1j}^e & \theta_{2j}^e & \dots & \theta_{mj}^e\end{bmatrix}^\top \in \mathbb{R}^m$ given by

$$\theta_j^e = \left(\boldsymbol{\Phi}_j^T \boldsymbol{\Phi}_j\right)^{-1} \boldsymbol{\Phi}_j^T \bar{e}_j. \tag{17}$$

Proof. Consider the error signal $e_j(\alpha)$, parameterized as

$$e_j(\alpha) = \begin{bmatrix}\phi_1(\alpha) & \phi_2(\alpha) & \dots & \phi_m(\alpha)\end{bmatrix} \hat{\theta}_j^e, \tag{18}$$

such that $\bar{e}_j$ is given by

$$\bar{e}_j = \boldsymbol{\Phi}_j \hat{\theta}_j^e. \tag{19}$$

Substituting this in (17) yields

$$\theta_j^e = \left(\boldsymbol{\Phi}_j^T \boldsymbol{\Phi}_j\right)^{-1} \boldsymbol{\Phi}_j^T \boldsymbol{\Phi}_j \hat{\theta}_j^e. \tag{20}$$

From this it follows that if and only if the matrix $\boldsymbol{\Phi}_j^T \boldsymbol{\Phi}_j$ is full rank, i.e., $\text{rank}(\boldsymbol{\Phi}_j^T \boldsymbol{\Phi}_j) = m$, then $\theta_j^e = \hat{\theta}_j^e$. This shows that if and only if $\text{rank}(\boldsymbol{\Phi}_j^T \boldsymbol{\Phi}_j) = \text{rank}(\boldsymbol{\Phi}_j^T) = m$, an exact reconstruction of the error signal can be made. Since the matrix $\boldsymbol{\Phi}$ is constructed from m linearly independent basis functions, the constraint $\text{rank}(\boldsymbol{\Phi}) = m$ is met if and only if there are $N \geq m$ measurement instances. This completes the proof. □

Theorem 5 allows defining the updated waveforms directly in terms of the parameters θ_j^u, as shown in the next section.

4.4. Waveform update

The signal $u_j(\alpha)$ that follows from the learning update is used to enhance the waveforms for the shear piezo elements, $s_1(\alpha)$ and $s_2(\alpha)$. The main constraint for the waveforms $s_1(\alpha)$ and $s_2(\alpha)$ is periodicity with a period of 2π, which is required to achieve periodic walking. However, the basis functions ϕ_i may be non-periodic. An example of basis function that is non-periodic with a period of 2π is an affine function, i.e.,

$$\phi(\alpha) = \alpha, \alpha \in [0, 2\pi). \tag{21}$$

This basis function can be used to compensate for the difference in slope between the mover position and the reference shown in Fig. 6, or to compensate effects of drift when those are still visible in the error. Other types of non-periodic basis functions are the radial basis functions used in [6]. However, the periodic extension of non-periodic basis functions leads to a discontinuous signal, see Fig. 8, and therefore a specific implementation is required.

An example of a basis function that is periodic with 2π is

$$\phi(\alpha) = \sin(\alpha). \tag{22}$$

Through this basis function, in combination with its higher harmonics, i.e., $\sin(i\pi), i \in \mathbb{N}$, and their counterparts $\cos(i\pi), i \in \mathbb{N}$, all periodic disturbances with a period of 2π can be captured.

Because of the periodicity constraint of the waveforms, the set of basis functions ϕ_i with corresponding θ_{j+1}^u, $i \in \{1, \dots, m\}$ is first divided into functions that are periodic with respect to the commutation angle with period 2π, given by $\phi_i^p(\alpha)$, $i \in \{1, \dots, m_p\}$, and functions that are non-periodic, given by $\phi_j^{np}(\alpha)$ $j \in \{1, \dots, m - m_p\}$. Using this division, $u_{j+1}(\alpha)$ is given by

$$\begin{aligned} u_{j+1}(\alpha) &= \begin{bmatrix}\phi_1^p(\alpha) & \dots & \phi_{m_p}^p(\alpha)\end{bmatrix} \theta_{j+1}^p \\ &\quad + \begin{bmatrix}\phi_1^{np} & \dots & \phi_{m-m_p}^{np}\end{bmatrix} \theta_{j+1}^{np} \end{aligned} \tag{23}$$

The interval where a shear group is not in contact with the mover is exploited to transform the non-periodic functions $\phi_j^{np}(\alpha)$ into continuous periodic signals $\delta s_{1,i}$ and $\delta s_{2,i}$, for respectively shear group 1 and shear group 2. In the regions where both shear groups are in contact with the mover, the signals $\delta_{1,i}$ and $\delta_{2,i}$ should satisfy

$$\frac{\partial \delta_{1,i}(\alpha)}{\partial \alpha} = \frac{\partial \phi_i^{np}(\alpha)}{\partial \alpha}, \tag{24}$$

$$\frac{\partial \delta_{2,i}(\alpha)}{\partial \alpha} = \frac{\partial \phi_i^{np}(\alpha)}{\partial \alpha}. \tag{25}$$

The regions where a shear group is not in contact with the mover are used to retract the shear such that a continuous waveform is obtained, i.e, such that the following is satisfied.

$$\delta_{1,i}(0) = \delta_{1,i}(2\pi),\ \delta_{2,i}(0) = \delta_{2,i}(2\pi), i,\ \{1, 2\}. \tag{26}$$

For the non-periodic basis function (21) this leads to functions $\delta_1(\alpha)$ and $\delta_2(\alpha)$ as shown in Fig. 9.

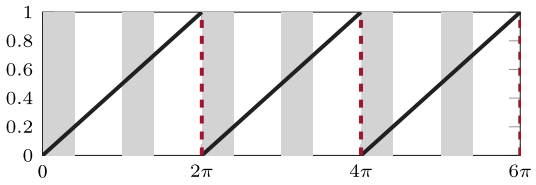

Fig. 8. Periodic extension of the basis function (21).

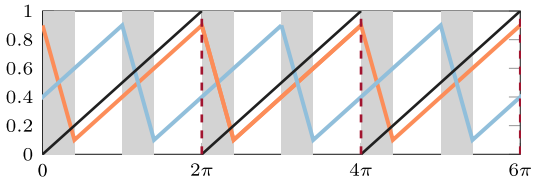

Fig. 9. Functions $\delta_1(\alpha)$ (—) and $\delta_2(\alpha)$ (—) corresponding to the non-periodic basis function (21). The discontinuous periodic extension of (21) is given by (—).

Applying this procedure to all non-periodic basis functions allows for a direct parameterization of the waveforms in terms of θ^{p}_{j+1} and θ^{np}_{j+1}, given by

$$\begin{aligned} &s_{1,j+1}(\alpha) \\ &= s_1(\alpha) + \sum_{i=1}^{m_p} \theta^{p}_{i,j+1}\phi^{p}_{i}(\alpha) + \sum_{j=1}^{m-m_p} \theta^{np}_{i,j+1}\delta_{1,i}(\alpha) \\ &s_{2,j+1}(\alpha) \\ &= s_2(\alpha) + \sum_{i=1}^{m_p} \theta^{p}_{i,j+1}\phi^{p}_{i}(\alpha) + \sum_{j=1}^{m-m_p} \theta^{np}_{i,j+1}\delta_{2,i}(\alpha). \end{aligned} \tag{27}$$

Remark 6. The reset of the shear elements allows for a continuous periodic extension of the non-periodic basis function and ensures that both periodic and non-periodic basis functions can be applied. The type of basis functions that is best suited depends on the disturbance that is compensated. The choice for periodic basis functions in this paper is motivated by Fig. 7, which shows that the error component e_{td} resembles a sine with a period of 2π. In addition, the non-periodic basis function (21) is used to compensate the slope difference between mover position and reference.

This completes Step 4 of Procedure 1, which is applied to an experimental setup in the next section.

5. Experimental results

In this section, the developed waveform optimization framework, i.e., Procedure 1, is applied to an experimental piezo stepper actuator.

5.1. Experimental setup

The experimental setup, as depicted in Fig. 1, is a piezo stepper actuator with the piezo configuration shown in Fig. 2. The piezoelectric material in this actuator is lead zirconate titanate (PZT). The input to the actuator is a voltage in the range $[-250, 250]$ V. The piezoelectric actuator is connected to a mover, which is connected to a parallel guide within a frame. The mover position is measured by a sincos encoder with a period length of $0.5 \cdot 10^{-6}$ m, and a 16-bit digital-analog converter.

5.2. Basis function selection

Since the error signal is sampled non-equidistantly in the α-domain for varying drive frequencies, the continuous error signal is reconstructed by mapping the measured error samples to a set of basis functions, as described in Section 4.3. The basis functions are selected based on the structure of the error shown in Fig. 6. First, a non-periodic basis function is used to compensate the slope of the error, given by

$$\phi^{np}_{1}(\alpha) = \alpha. \tag{28}$$

Next, it is observed that the main component of the trendline deviation e_{td} in Fig. 7 is periodic, with a fundamental harmonic with a period of 2π. A set of basis functions is chosen that can capture the first 100 harmonics of this disturbance, i.e.,

$$\phi^{p}_{i}(\alpha) = \sin(i\alpha), \quad \phi^{p}_{M+i}(\alpha) = \cos(i\alpha), \tag{29}$$

$i \in \{1, \dots, M\}$, with $M = 100$.

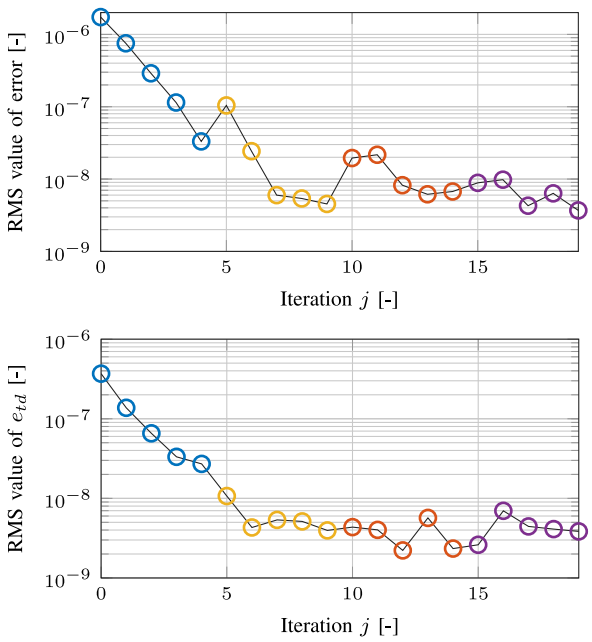

Fig. 10. Convergence of the RMS value of the error (top) and the trendline deviation e_{td} (bottom) during open-loop walking experiments. Monotonic convergence of the RMS of e_{td} is observed while varying the step frequency, but due to rate-dependency the RMS of the error increases when the step frequency changes. Subsequent step frequencies: 1 Hz (○), 10 Hz (○), 21 Hz (○), 17 Hz (○).

5.3. Experimental results

Procedure 1 is applied to the experimental setup depicted in Fig. 1 using the set of basis functions (29). The desired linear relation between the commutation angle α and the mover position is described by the reference $y_d(\alpha) = 3 \cdot 10^{-7}\alpha$. The applied step frequencies range between 1–21 Hz.

In Fig. 10 (top), the root mean square, $\text{RMS}(e_j) = \frac{1}{N_j}\sum_{k=1}^{N_j} e_j(\bar{\alpha}_k)^2$, of the error signals over iterations is given. This figure shows that the RMS value converges to a bounded region, even though the step frequency varies over iterations. The non-equidistantly sampled signals are mapped to the set of basis functions, and the waveform that is learned can be applied at different step frequencies. However, when the step frequency changes, there is an increase in error due to rate-dependent behavior. This is illustrated in Figs. 10 (bottom) and 11, which show that this increase in error is due to a change in slope. Fig. 11, also shows that a significant performance improvement is obtained with respect to the error observed at iteration $j = 0$. The enhanced waveforms for iteration $j = 20$ are depicted in Fig. 12, cf. Fig. 4.

In Fig. 13, convergence of the RMS value of the error is shown for experiments with step frequencies ranging between 1–8 Hz, for experiments with and without hysteresis compensation. The hysteresis compensation according to [15] results in a smaller initial error, but for later iterations it is shown that this part of the hysteresis can be compensated through learning the waveforms as well. Since this hysteresis compensation does not take into account the rate-dependency, the change in error slope when the step frequency changes remains.

Remark 7. When the α-domain ILC algorithm is running long-term during standard operation of a system, i.e., when the number of iterations is high, it automatically corrects for disturbances such as temperature fluctuations and varying friction components, since these variations typically occur on a much larger timescale than the ILC updates. Satisfying the monotonic convergence condition in Theorem 4 ensures good learning transients, such that the error will not grow over iterations [17].

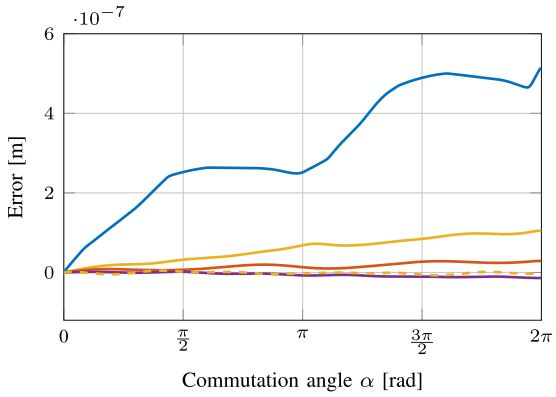

Fig. 11. Error signals for iterations 0 (1 Hz, ——), 5 (10 Hz, ——), 9 (10 Hz, - - -) 10 (21 Hz, ——), 15 (17 Hz, ——). The increase in error between iterations 9 and 10 is mostly due to a rate-dependent change in slope.

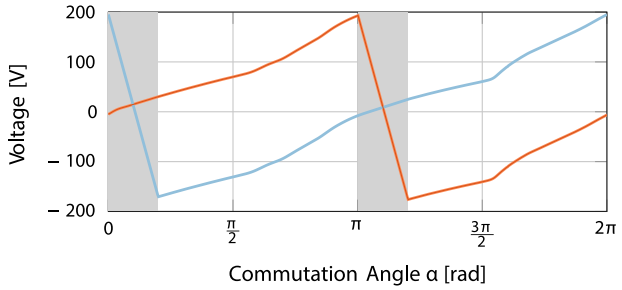

Fig. 12. Enhanced waveforms $s_{1,20}(\alpha)$ (——) and $s_{2,20}(\alpha)$ 2 (——) obtained at iteration $j = 20$. Regions where only one shear group is in contact with the mover are indicated in gray.

6. Conclusion

The presented framework can perfectly compensate commutation-angle domain disturbances for systems with static dynamics. This approach is successfully applied to piezo stepper actuators that exhibit repeating disturbances introduced by the walking behavior in the commutation angle domain. Other applications that may benefit from this approach include permanent magnet motors with cogging. The presented framework is capable of fully mitigating repeatable disturbances in the α-domain for a piezo stepper actuator while coping with iteration-varying and non-equidistant measurement and actuation points. Basis functions are used to parameterize the input and error signals and obtain continuous descriptions. These continuous descriptions are used in an update law. Compensation of the α-domain repeating disturbances for a piezo stepper actuator during walking experiments results in a linear relation between commutation angle and mover position. This improves the positioning accuracy and reduces the complexity of closed-loop control in an industrial setting. Future research will consider further compensation of hysteresis and rate-dependent effects.

CRediT authorship contribution statement

Leontine Aarnoudse: Conceptualization, Writing – review & editing, Software, Validation, Investigation, Writing – original draft. **Nard Strijbosch:** Conceptualization, Writing – review & editing, Software, Validation, Investigation, Writing – original draft. **Paul Tacx:** Conceptualization, Writing – review & editing, Software. **Edwin Verschueren:** Conceptualization, Writing – review & editing, Supervision. **Tom Oomen:** Conceptualization, Writing – review & editing, Supervision.

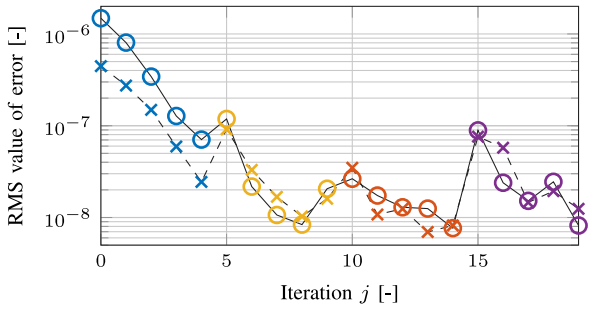

Fig. 13. Convergence of the RMS value of the error, with (- - -, ×) and without (——, ○) hysteresis compensation. Subsequent step frequencies: 1 Hz (——), 5 Hz (——), 8 Hz (——), 3 Hz (——).

Declaration of competing interest

The authors declare that they have no known competing financial interests or personal relationships that could have appeared to influence the work reported in this paper.

Data availability

No data was used for the research described in the article.

References

[1] Merry RJE, Maassen MGJM, Van De Molengraft MJG, Van De Wouw N, Steinbuch M. Modeling and waveform optimization of a nano-motion piezo stage. IEEE/ASME Trans Mechatronics 2011;16(4):615–26.
[2] Den Heijer M, Fokkema V, Saedi A, Schakel P, Rost MJ. Improving the accuracy of walking piezo motors. Rev Sci Instrum 2014;28:055007.
[3] Shamoto E, Moriwaki T. Development of a "walking drive" ultraprecision positioner. Precis Eng 1997;20(2):85–92.
[4] Uzunovic T, Golubovic E, Sabanovic A. Piezo LEGS driving principle based on coordinate transformation. IEEE/ASME Trans Mechatronics 2015;20(3):1395–405.
[5] Kusakawa T, Torii A, Doki K, Ueda A. Control waveforms applied to piezo elements used in a miniature robot. In: Micro-nanomechatronics hum. sci. 2004 fourth symp. micro-nanomechatronics information-based soc. 2004. 2004, p. 307–12.
[6] Aarnoudse L, Strijbosch N, Verschueren E, Oomen T. Commutation-angle iterative learning control for intermittent data: Enhancing piezo-stepper actuator waveforms. In: IFAC 21st world congr.. Berlin, Germany; 2020.
[7] Jiang TY, Ng TY, Lam KY. Optimization of a piezoelectric ceramic actuator. Sensors Actuators A 2000;84(1):81–94.
[8] Van Brussel H, Reynaerts D, Vanherck PI, Versteyhe M, Devos S. A nanometre-precision, ultra-stiff piezostepper stage for ELID-grinding. CIRP Ann 2003;52(1):317–22.
[9] Hoelzle DJ, Barton KL. On spatial iterative learning control via 2-D convolution: Stability analysis and computational efficiency. IEEE Trans Control Syst Technol 2016;24(4):1504–12.
[10] Kong FH, Boudali AM, Manchester IR. Phase-indexed ILC for control of underactuated walking robots. In: 2015 IEEE conf. control appl.. Sydney, Australia; 2015, p. 1467–72.
[11] Mooren N, Witvoet G, Oomen T. Gaussian process repetitive control for suppressing spatial disturbances. IFAC-PapersOnLine 2020;53(2):1487–92.
[12] Strijbosch N, Tacx P, Verschueren E, Oomen T. Commutation angle iterative learning control: Enhancing piezo-stepper actuator waveforms. In: 8th IFAC symp. mechatron. syst.. Vienna, Austria; 2019, p. 1451–6.
[13] Leang KK, Zou Q, Devasia S. Feedforward control of piezoactuators in atomic force microscope systems: Inversion-based compensation for dynamics and hysteresis. IEEE Control Syst 2009;29(1):70–82.
[14] Fleming AJ, Leang KK. Design, modeling and control of nanopositioning systems. Springer; 2014.

[15] Strijbosch N, Tiels K, Oomen T. Hysteresis feedforward compensation: A direct tuning approach using hybrid-MEM-elements. IEEE Control Syst Lett 2022;6:1070–5.
[16] Bristow DA, Tharayil M, Alleyne AG. A survey of iterative learning control. IEEE Control Syst 2006;26(3):96–114.
[17] Longman RW. Iterative learning control and repetitive control for engineering practice. Internat J Control 2000;73(10):930–54.

Leontine Aarnoudse received the B.Sc. degree (2017) and M.Sc. degree (cum laude) (2019) in Mechanical Engineering from the Eindhoven University of Technology, Eindhoven, The Netherlands. She is currently pursuing a Ph.D. degree in the Control Systems Technology group within the department of Mechanical Engineering at Eindhoven University of Technology. Her research interests are in the field of control for precision mechatronics, and are mostly centered around the development of learning theory for these systems.

Nard Strijbosch received his B.Sc. degree (cum laude), M.Sc. degree (cum laude) and Ph.D. degree (2022) from the Eindhoven University of Technology, Eindhoven, The Netherlands. He is currently a system engineer at IBS Precision Engineering. He is a recipient of the IEEJ Industry Applications Society Excellent Presentation Award (SAMCON 2018). His research interest is in the field of motion control and learning control techniques for applications in mechatronic systems.

Paul Tacx received the M.Sc. degree (cum laude) in mechanical engineering from the Eindhoven University of Technology, Eindhoven, the Netherlands, in 2019, where he is currently pursuing the Ph.D. degree with the Control Systems Technology Group. His research interests include identification for advanced motion control and control of complex mechatronic systems.

Edwin Verschueren is Senior Mechatronics Engineer at Thermo Fisher Scientific within the Materials and Structural Analysis division. He holds the position of competence owner on mechatronic systems design. He received his M.Sc. degree in 1996 from Eindhoven University of Technology, Eindhoven and started working for ASML as mechatronics engineer. He continued his profession from 2001 until now at Thermo Fisher Scientific (formerly FEI Company) and during his career he was responsible for the design and market introduction of mechatronic modules for electron microscopes (sample manipulation stages, apertures mechanisms and sample loaders). Key aspects of his work are evaluation and integration of innovative technologies into solutions for high precision sample manipulation. His interests are in the field of physical modeling, actuator and sensor technologies and control algorithm design.

Tom Oomen is full professor with the Department of Mechanical Engineering at the Eindhoven University of Technology. He is also a part-time full professor with the Delft University of Technology. He received the M.Sc. degree (cum laude) and Ph.D. degree from the Eindhoven University of Technology, Eindhoven, The Netherlands. He held visiting positions at KTH, Stockholm, Sweden, and at The University of Newcastle, Australia. He is a recipient of the 7th Grand Nagamori Award, the Corus Young Talent Graduation Award, the IFAC 2019 TC 4.2 Mechatronics Young Research Award, the 2015 IEEE Transactions on Control Systems Technology Outstanding Paper Award, the 2017 IFAC Mechatronics Best Paper Award, the 2019 IEEJ Journal of Industry Applications Best Paper Award, and recipient of a Veni and Vidi personal grant. He is currently a Senior Editor of IEEE Control Systems Letters (L-CSS) and Associate Editor of IFAC Mechatronics, and he has served on the editorial boards of the IEEE Control Systems Letters (L-CSS) and IEEE Transactions on Control Systems Technology. He has also been vice-chair for IFAC TC 4.2 and a member of the Eindhoven Young Academy of Engineering. His research interests are in the field of data-driven modeling, learning, and control, with applications in precision mechatronics.